GEOPHYSICS, VOL. 76, NO. 4 (JULY-AUGUST 2011); P. T79–T89, 14 FIGS., 6 TABLES.
10.1190/1.3587223

Finite-difference modeling with adaptive variable-length spatial operators

Yang Liu[1] and Mrinal K. Sen[2]

ABSTRACT

Most finite-difference simulation algorithms use fixed-length spatial operators to compute spatial derivatives. The choice of length is dictated by computing cost, stability, and dispersion criteria that are satisfied globally. We propose finite-difference schemes with adaptive variable-length spatial operators to decrease computing costs significantly without reducing accuracy. These schemes adopt long operators in regions of low velocity and short operators in regions of high velocity. Two methods automatically determine variable operator lengths. Dispersion analysis, along with 1D and 2D modeling, demonstrates the validity and efficiency of our schemes. In addition, a hybrid absorbing boundary condition helps reduce unwanted reflections from model boundaries. Our scheme is more efficient than those based on variable-grid methods for modeling, migration, and inversion of models with complex velocity structures because the latter require local grid refinement, which usually increases memory requirements and computing costs.

INTRODUCTION

Finite-difference (FD) methods are preferred over numerical methods such as finite-element and pseudospectral schemes in seismic modeling (e.g., Kelly et al., 1976; Virieux, 1984; Holberg, 1987; Robertsson et al., 1994; Igel et al., 1995; Etgen and O'Brien, 2007; Bansal and Sen, 2008), migration (e.g., Claerbout, 1985; Larner and Beasley, 1987; Li, 1991; Ristow and Ruhl, 1994; Zhang et al., 2000; Fei and Liner, 2008), and inversion (e.g., Pratt et al., 1998; Ravaut et al., 2004; Abokhodair, 2009) because of their efficient use of memory, low computing cost, and ease of implementation. However, compared with ray theory, Gaussian beam theory, and wavenumber integral methods, FD methods are still more expensive computationally. An ever-present challenge is to increase their efficiency without decreasing accuracy, to increase accuracy without decreasing efficiency, or to increase efficiency and accuracy.

Several variants of FD methods improve accuracy and efficiency. These schemes include variable grids (Wang and Schuster, 1996; Hayashi and Burns, 1999), discontinuous grid (Aoi and Fujiwara, 1999), irregular grids (Opršal and Zahradník, 1999), staggered grids (e.g., Madariaga, 1976; Virieux, 1986; Graves, 1996; Robertsson, 1996; Bohlen and Saenger, 2006), rotated staggered grids (Saenger et al., 2000; Krüger et al., 2005; Bansal and Sen, 2008), variable time steps (Tessmer, 2000), and implicit FD (Emerman et al., 1982; Lele, 1992; Ristow and Ruhl, 1997; Liu and Sen, 2009a, 2009b). The key idea behind variable, discontinuous, or irregular grid methods is to adopt small grids in low-velocity regions and large grids in high-velocity regions. These methods, in principle, improve accuracy with a small increase in computing costs. However, as a result of difficulties inherent in automatically gridding complex velocity models, they have not been used widely.

High-order FDs usually are applied to increase accuracy and reduce dispersion (e.g., Dablain, 1986; Hestholm, 2009; Liu and Sen, 2009a, 2009b, 2009c). Generally, FD coefficients are determined by a Taylor series expansion (e.g., Dablain, 1986; Fornberg, 1998) or by optimization (e.g., Fornberg, 1987; Kindelan et al., 1990; Jastram and Behle, 1993). Most FD methods determine spatial FD operators only in the space domain (e.g., Dablain, 1986; Liu and Sen, 2009a, 2009b). However, the seismic wave-propagation calculation is done in the space and time domains. If these operators are used directly to solve the wave equations, a potentially large dispersion will always exist. It has been proven that modeling accuracy is second order when conventional $2M$th-order spatial FD and second-order temporal FD stencils are used directly to solve the acoustic wave equation (Liu and Sen, 2009c).

Manuscript received by the Editor 30 October 2010; revised manuscript received 22 January 2011; published online 3 June 2011.
[1]China University of Petroleum, State Key Laboratory of Petroleum Resources and Prospecting, Beijing, China. E-mail: wliuyang@vip.sina.com.
[2]The University of Texas at Austin, Institute for Geophysics, Austin, Texas, U.S.A. E-mail: mrinal@ig.utexas.edu.

To deal with the issue, a unified methodology has been proposed to derive spatial FD coefficients in the joint time-space domain to reduce numerical dispersion (Finkelstein and Kastner, 2007, 2008). The key idea of this method is that the dispersion relation is completely satisfied at several designated frequencies. This new time-space-domain FD method has been developed further for 1D, 2D, and 3D acoustic-wave modeling using a plane-wave theory and Taylor-series expansion (Liu and Sen, 2009c). Under the same spatial discretization, the new 1D method can reach $2M$th-order accuracy and is always stable. The 2D method can reach $2M$th-order accuracy along eight directions and has better stability. We have extended the method to solve acoustic vertical transversely isotropic (VTI) equations (Liu and Sen, 2010a).

In practice for heterogeneous models, FD operator designs are based on the minimum velocity; fixed FD operators are used for regularly discretized grids. Because the main frequency of the source is usually fixed in the modeling, the wavelength in a lower-velocity medium is smaller than the wavelength in a higher-velocity medium. For fixed grid size and time step, when the same FD operators are used in heterogeneous media modeling, accuracy of wave propagation in a higher-velocity medium is greater than that in a lower-velocity medium. Long FD operators provide greater accuracy than short FD operators. Therefore, we can use long FD operators for low velocities and short FD operators for high velocities.

In this paper, based on the time-space-domain dispersion-relation-based FD method (Liu and Sen, 2009c), we propose FD schemes with variable FD operator lengths. Their validity and efficiency are demonstrated by dispersion analysis and by 1D and 2D modeling examples.

METHOD AND DISPERSION ANALYSIS

For a fixed grid size and fixed time step, when the same-length FD operator is used for numerical modeling in a heterogeneous model, we attain greater accuracy in higher-velocity grids than in lower-velocity grids. Here, we demonstrate this using an 1D acoustic wave equation.

The 1D acoustic wave equation is given by

$$\frac{\partial^2 p}{\partial x^2} = \frac{1}{V^2}\frac{\partial^2 p}{\partial t^2}, \tag{1}$$

where $p = p(x,t)$ is a scalar wavefield and V is the velocity.

The following second-order temporal FD and $2M$th-order spatial FD schemes are usually used:

$$\frac{\partial^2 p}{\partial t^2} = \frac{1}{\tau^2}\left[-2p_j^i + \left(p_j^{i-1} + p_j^{i+1}\right)\right] \tag{2}$$

and

$$\frac{\partial^2 p}{\partial x^2} = \frac{1}{h^2}\left[a_0 p_j^i + \sum_{m=1}^{M} a_m\left(p_{j-m}^i + p_{j+m}^i\right)\right], \tag{3}$$

where

$$a_0 = -2\sum_{m=1}^{M} a_m, \tag{4}$$

$p_j^i = p(jh, i\tau)$, a_m are spatial FD coefficients, h is the grid size, τ is the time step, and FD operator length is $2M+1$. Substituting equations 2 and 3 into equation 1, we have the following recursion formula:

$$p_j^{i+1} = 2p_j^i - p_j^{i-1} + r^2\left[a_0 p_j^i + \sum_{m=1}^{M} a_m\left(p_{j-m}^i + p_{j+m}^i\right)\right], \tag{5}$$

where $r = v\tau/h$. Conventional space-domain dispersion-relation-based spatial FD coefficients only make the recursion formula 5 of FD modeling reach second-order accuracy, so we adopt the following time-space-domain dispersion-relation-based FD coefficients to reach $2M$th-order accuracy (Liu and Sen, 2009c):

$$a_m = \frac{(-1)^{m+1}}{m^2}\prod_{1\le n\le M, n\ne m}\left|\frac{n^2 - r^2}{n^2 - m^2}\right| \quad (m = 1, 2, ..., M), \tag{6}$$

where a_m reduce to conventional spatial FD coefficients when setting $r = 0$ in equation 6. Unlike the coefficients used in conventional schemes, the spatial FD coefficients 6 are dependent on the Courant number.

The parameter δ is defined to describe the grid dispersion in FD modeling:

$$\delta = \frac{V_{\mathrm{FD}}}{V}, \tag{7}$$

where V_{FD} is FD propagation velocity, determined by

$$V_{\mathrm{FD}} = \frac{\tilde{\omega}}{k}, \tag{8}$$

with $\tilde{\omega}$ the dispersion frequency determined by the dispersion relation from equation 5 and k the wavenumber. For 1D modeling, using the plane-wave theory, equations 5 and 7 (the plane-wave theory is independent on equations 5 and 7), we obtain (Liu and Sen, 2009c)

$$\delta = \frac{2}{rkh}\sin^{-1}\sqrt{r^2\sum_{m=1}^{M} a_m \sin^2\left(\frac{mkh}{2}\right)}. \tag{9}$$

If δ equals one, then there is no dispersion. If δ is much greater or less than one, a large dispersion will occur. Because $kh = \pi$ at the Nyquist frequency, kh only ranges from zero to π when calculating δ.

Figure 1a shows the variation of the dispersion parameter δ with kh for different velocities and the same M. One can see that the dispersion curves are nearly the same for different velocities.

Note the exact dispersion relation is

$$kh = \frac{\omega h}{V} = \frac{2\pi f h}{V}, \tag{10}$$

where ω is angular frequency. Then

$$f = \frac{V}{2\pi h}kh. \tag{11}$$

When kh ranges from zero to π, f changes from zero to $V/(2h)$. For example, when $h = 20$ m, maximum values of f are 37.5,

62.5, 87.5, and 112.5 Hz for $V = 1500$, 2500, 3500, and 4500 m/s, respectively, which means that maximum frequency increases with velocity increase for fixed grid size. Then kh can be transformed into f easily; thus, Figure 1a is changed into Figure 1b.

From Figure 1b, it follows that the dispersion for high-frequency components reduces with the increase of velocity for fixed M and h. Note that source frequency in the modeling is predetermined and usually is related to the minimum velocity for fixed grid size. For instance, the maximum frequency must be less than or equal to 37.5 Hz for a grid size of 20 m with a minimum velocity of 1500 m/s. Therefore, we can shorten the FD operators for the higher-velocity grids to decrease the accuracy and obtain nearly the same accuracy as the long FD operators for the low-velocity grids.

We define the difference between FD propagation time and exact propagation time through one grid to describe FD error, i.e.,

$$\varepsilon = \frac{h}{V_{\mathrm{FD}}} - \frac{h}{V} = \frac{h}{V}\left(\frac{V}{V_{\mathrm{FD}}} - 1\right), \qquad (12)$$

where V_{FD} is FD propagation phase velocity determined by equation 8. Substituting equation 7 into equation 12, we have

$$\varepsilon = \frac{h}{V}\left(\delta^{-1} - 1\right). \qquad (13)$$

Note that ε approximately represents propagation time error of one grid. Thus, if ε equals zero, there is no dispersion; when ε is much greater or less than zero, large dispersion will occur. Also note that δ is related to M and f. Therefore, ε is a function of V, M, and f. Using equation 13, Figure 1b changes into Figure 1c, showing variation of dispersion $\log_{10}|\varepsilon|$ with f.

Method 1

Next, we propose two methods to determine variable FD operator lengths. For the first method, the following inequality can be used to attain nearly the same accuracy for different velocities:

$$|\varepsilon(V,M,f)| \le \xi = |\varepsilon(V_{\min}, L_{\min}, f)| \text{ when } f \le f_{\max}, \qquad (14)$$

where M is the FD operator length parameter and $L_{\min}$ is the value of M for the minimum velocity $V_{\min}$ of all involved grids. Using this criterion, minimum values of M can be determined for different velocities.

Figure 2 shows dispersion curves for different FD operator lengths and different velocities with method 1. In this figure, $V = 1500$, 2500, 3500, and 4500 m/s; $\tau = 0.001$ s; $h = 20$ m; $V_{\min} = 1500$ m/s; and $L_{\min} = 20$. The values of M are determined by equation 14 and are 20, 12, 10, and 8 for the four different velocities. Figure 2 demonstrates that short FD operators may be adopted for high-velocity regions to obtain an accuracy that is greater than or equal to the accuracy of the long FD operators for low-velocity regions.

Method 2

For the given maximum frequency $f_{\max}$ and maximum error η, the following inequality is satisfied:

$$|\varepsilon(V,M,f)| \le \eta \text{ when } f \le f_{\max}. \qquad (15)$$

The FD operators for high-velocity regions can be shortened further than with method 1.

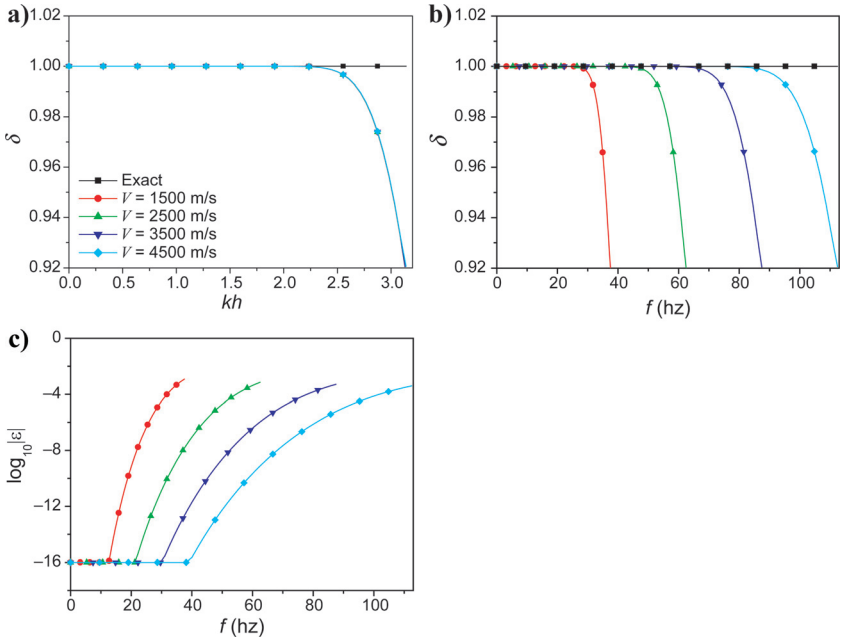

Figure 1. Plot of 1D dispersion curves for the same FD operator length and different velocities. (a) Variation of dispersion δ with kh, (b) variation of dispersion δ with f, (c) variation of dispersion $\log_{10}|\varepsilon|$ with f. Here, $V = 1500$, 2500, 3500, and 4500 m/s; $\tau = 0.001$ s; $h = 20$ m; and $M = 20$. We set $\log_{10}|\varepsilon| = -16$ when $|\varepsilon| < 10^{-16}$.

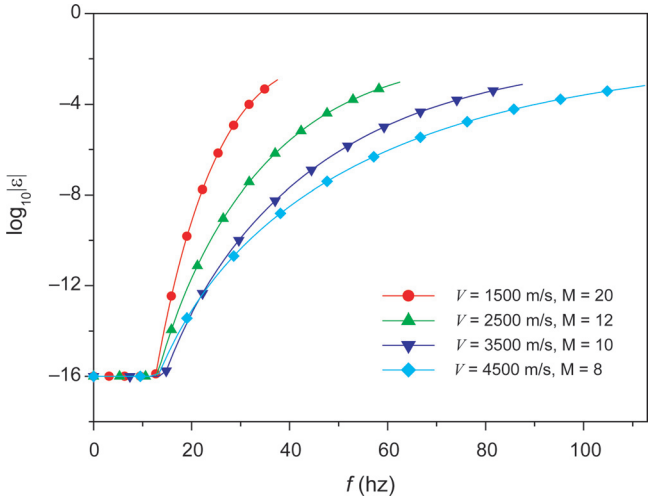

Figure 2. Plot of 1D dispersion curves for different FD operator lengths and velocities with our method 1. Here, $V = 1500$, 2500, 3500, and 4500 m/s; $\tau = 0.001$ s; $h = 20$ m; $L_{\min} = 20$; and $M = 20$, 12, 10, and 8, as determined by method 1. We set $\log_{10}|\varepsilon| = -16$ when $|\varepsilon| < 10^{-16}$.

Figure 3 shows dispersion curves for different FD operator lengths and different velocities with method 2. In this figure, $V = 1500$, 2500, 3500, and 4500 m/s; $\tau = 0.001$ s; $h = 20$ m; $\eta = 10^{-9}$; and $f_{max} = 20$ Hz. Using equation 15, we obtain $M = 20$, 9, 6, and 5 for the four different velocities.

Figure 4 displays FD operator lengths for different velocities and operator lengths of minimum velocity using method 1. Figure 5 gives FD operator lengths for different velocities and different maximum errors with method 2. These two figures show that operator lengths generally decrease with the increasing velocity, and operator lengths determined by method 2 for high velocities are shorter than those determined by method 1 when the same operator lengths for the minimum velocity are involved.

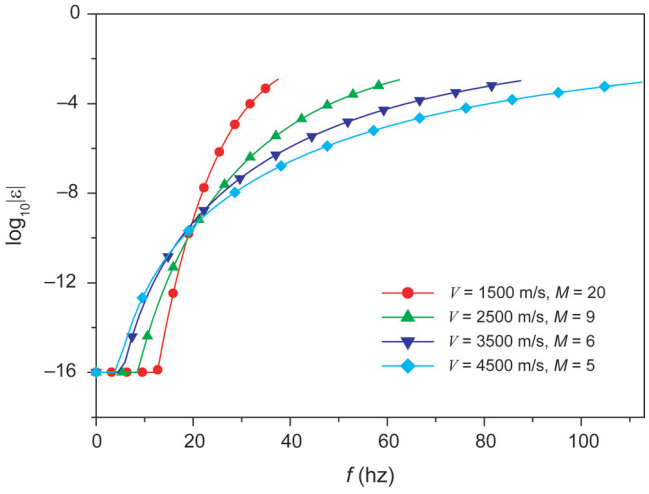

Figure 3. Plot of 1D dispersion curves for different FD operator lengths and velocities with method 2. Here, $V = 1500$, 2500, 3500, and 4500 m/s; $\tau = 0.001$ s; $h = 20$ m; $f_{max} = 20$ Hz; $\eta = 10^{-9}$; and $M = 20$, 9, 6, and 5, as determined by method 2. We set $\log_{10}|\varepsilon| = -16$ when $|\varepsilon| < 10^{-16}$.

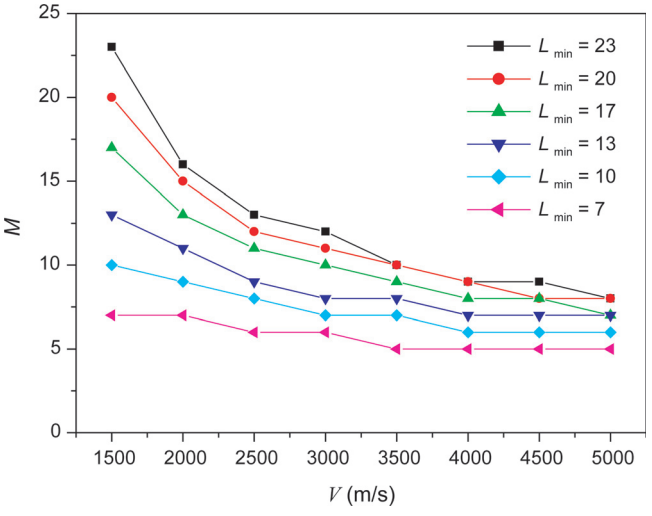

Figure 4. Plot of FD operator lengths for different velocities and operator lengths of minimum velocity with method 1. Here, $V = 1500$, 2000, 2500, 3000, 3500, 4000, 4500, and 5000 m/s; $\tau = 0.001$ s. $h = 20$ m; $L_{min} = 23$, 20, 17, 13, 10, and 7; and M are determined by method 1. We set $\log_{10}|\varepsilon| = -16$ when $|\varepsilon| < 10^{-16}$.

MODELING EXAMPLES

In the following modeling tests, we use method 2 to determine operator lengths. We show results from 1D and 2D modeling using fixed and variable FD operator length, and we compare their accuracy and computing speed (CPU time) to demonstrate feasibility and efficiency of our proposed variable-FD-operator-length method.

1D modeling

We use recursion equation 5 to perform 1D acoustic-wave modeling with the FD coefficients given in equation 6. For all 1D numerical modeling examples shown in this paper, we use the following initial conditions:

$$p(x,t)|_{t=0} = (x - x_0)e^{-(\alpha^2/4h^2)(x-x_0)^2}, \tag{16a}$$

$$\left.\frac{\partial p(x,t)}{\partial t}\right|_{t=0} = 0, \tag{16b}$$

where x_0 is the location of the source center and α^2 is an attenuation coefficient.

Figure 6 shows traces obtained by 1D modeling with fixed- and variable-FD-operator-length methods for an inhomogeneous model. Traces 1, 4, and 7 in Figure 6c are calculated by different fixed FD operators (length $2M+1$) for $M = 6$, 17, and 32, respectively. Traces 2, 5, and 8 are calculated by different variable FD operator lengths given in Table 1. Traces 3, 6, and 9 are the differences between traces 2 and 1, 5 and 4, and 8 and 7, respectively. Comparing traces 1, 4, and 7 with different fixed FD operator lengths and trace 10 of the reference solution, we

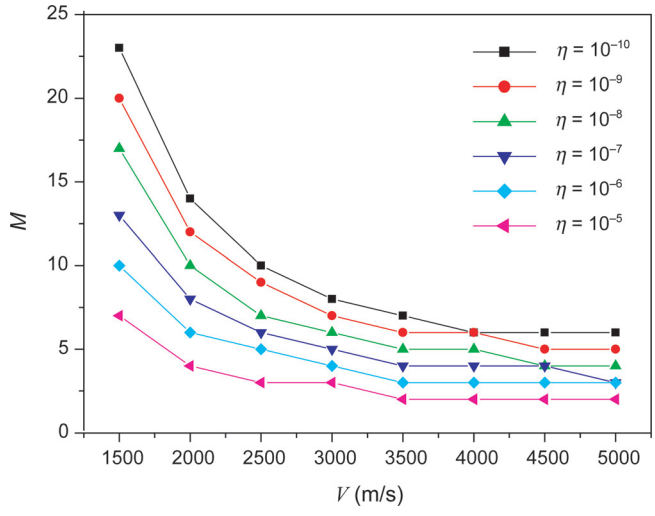

Figure 5. Plot of FD operator lengths for different velocities and maximum errors with method 2. Here, $V = 1500$, 2000, 2500, 3000, 3500, 4000, 4500, and 5000 m/s; $\tau = 0.001$ s; $h = 20$ m; $f_{max} = 20$ Hz; $\eta = 10^{-10}$, 10^{-9}, 10^{-8}, 10^{-7}, 10^{-6}, and 10^{-5}; and M are determined by method 2. We set $\log_{10}|\varepsilon| = -16$ when $|\varepsilon| < 10^{-16}$.

see that accuracy increases with increasing FD operator length. Trace 2, calculated from variable-FD-operator-length parameter M, equals six, five, and four for different velocities shown in Table 1. It seems nearly the same as trace 1 calculated from a fixed FD operator length of six. Trace 3, the difference between traces 1 and 2, also indicates they are nearly identical. This conclusion can likewise be drawn from traces 4–9.

Table 2 shows CPU times from the same computer (Lenovo ThinkPad T61 with an Intel T7300 Core 2 Duo processor and 2 GB of memory). Note that CPU time only includes the time of executing recursion equation 5; it does not include the time for reading and writing data, preparing FD coefficients, etc. From the table, one can see that the variable-length method requires less CPU time than a fixed-length method. Table 3 shows CPU time for different thicknesses of different velocities; this demonstrates that variable FD operator lengths for different velocities may be used to decrease the computing cost without significantly reducing the accuracy.

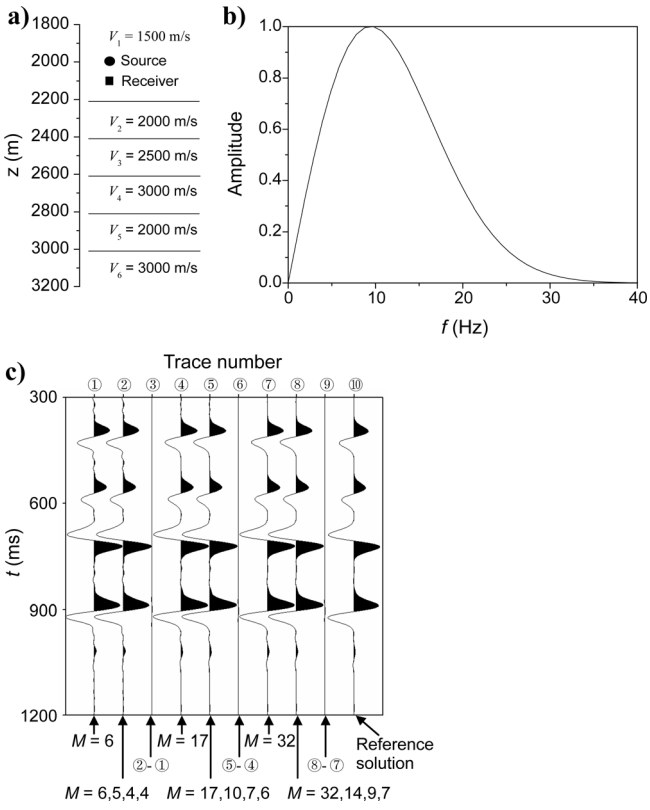

Figure 6. The 1D modeling records computed by FD methods with fixed and variable FD operator lengths for an inhomogeneous model. (a) Model, source, and receiver. The model has six layers and four velocities, where z represents depth. Model size is 4000 m, $h = 20$ m, and $\tau = 0.001$ s. (b) Amplitude spectrum of the analytic wavelet generated by initial conditions 16a and 16b, with $\alpha^2 = 1.25$. (c) Modeling records. The reference solution is generated by a second-order FD method with fine discretization. Generally, variation of FD order affects reflections from shallow layers more than those from deep layers.

2D modeling

We adopt the time-space-domain FD modeling method for the 2D acoustic-wave-equation modeling in which spatial FD coefficients are determined by the Courant number and the space point number (Liu and Sen, 2009c).

Table 2. CPU time of 1D FD modeling for the horizontal layered model in Figure 6a.

Type of FD length	Value of M	CPU time of 4000 recursion times (s)
Fixed	6	0.22
Variable	6, 5, 4, 4	0.20
Fixed	17	0.45
Variable	17, 10, 7, 6	0.37
Fixed	32	0.72
Variable	32, 14, 9, 7	0.52

Table 3. CPU time of 1D FD modeling for different thicknesses. Model parameters are shown in Figure 6a, except for thicknesses of layers 1 and 6. Values of $M = 32, 14, 9$, and 7 are used for four different velocities from Table 1.

Thickness (m)		CPU time of 4000 recursion times (s)	
Layer 1	Layer 6	Fixed-length method	Variable-length method
2000	1200	0.72	0.50
500	2700	0.72	0.31
100	3100	0.72	0.28

Table 1. The 1D FD operator length $2M + 1$ for different velocities and maximum frequencies used in Figure 6.

			M for different velocities			
Trace number	f_{max} (Hz)	η (s)	1500 m/s	2000 m/s	2500 m/s	3000 m/s
2	10	10^{-8}	6	5	4	4
5	20	10^{-8}	17	10	7	6
8	25	10^{-8}	32	14	9	7

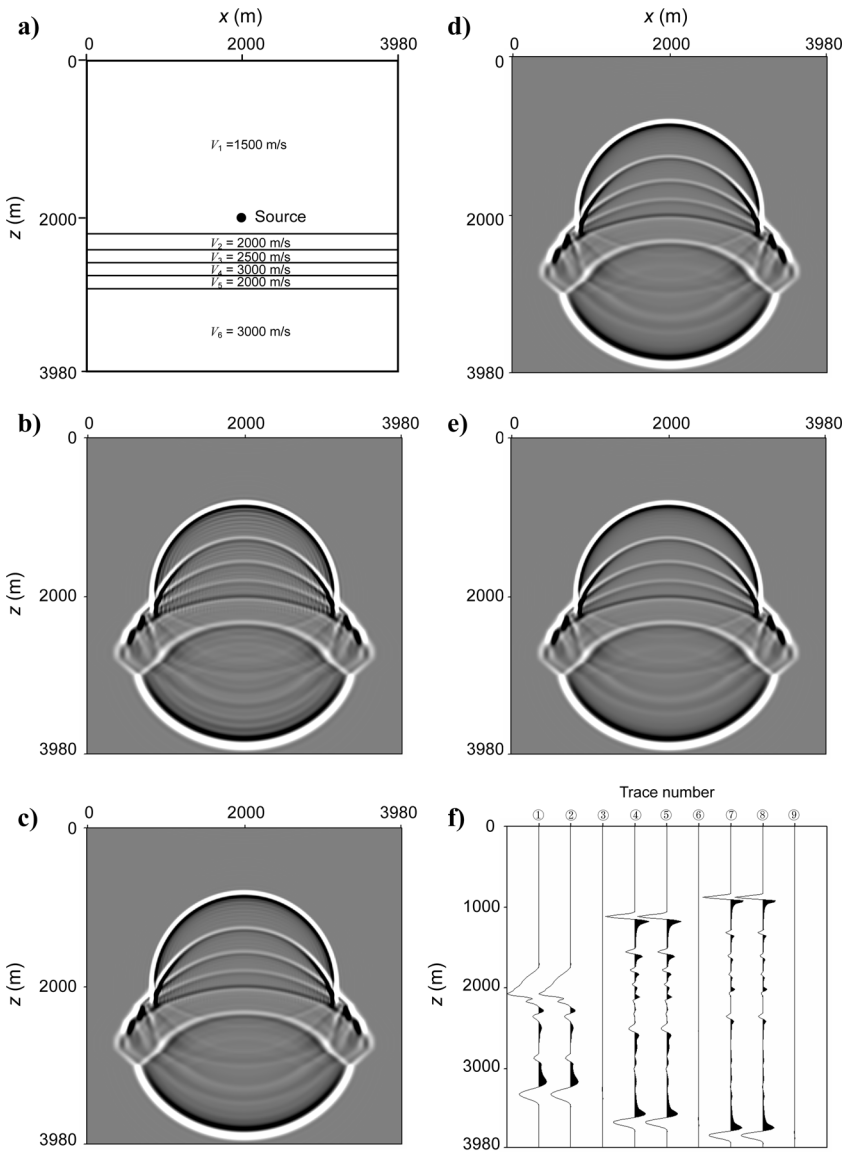

Figure 7. The 2D modeling snapshots at 800 ms computed by the FD methods, with fixed and variable FD operator lengths for a horizontally layered model. (a) Model parameters and source location. A one-period sine function with 20-Hz frequency is used to generate vibrations. (b-d) Snapshots computed by fixed-length FD operators, with $M = 7$, 14, and 34. (e) Snapshot computed by variable-length FD operators with $M = 34$, 10, 6, and 4 for four different velocities (see Table 4). (f) Comparison of some traces from (d) and (e). Traces 1, 4, and 7 are from (d); traces 2, 5, and 8 are from (e). The x-coordinates of traces 1–2, 4–5, and 7–8 are 800, 1200, and 1600 m, respectively. Traces 3, 6, and 8 are the differences between traces 1 and 2, traces 4 and 5, and traces 7 and 9, respectively.

The first example of 2D modeling is for a horizontally layered model. Figure 7 displays 2D snapshots computed by the FD methods with fixed and variable FD operator lengths. Model parameters and source location are given in Figure 7a, and FD operator lengths are shown in Table 4. Figure 7b, c, and d demonstrates that the dispersion reduces with the increase of FD operator length. Figure 7e, calculated by the FD method with variable FD operator length, is almost the same as Figure 7d, which is confirmed by Figure 7f; it displays the difference between Figure 7d and e. Computational efficiency of the variable-length method for this model is demonstrated by CPU time, shown in Table 5.

Table 6, showing CPU time for different thicknesses of different velocities, suggests that efficiency depends on the characteristics of the velocity model. The 2D modeling results suggest that variable FD operator lengths for different velocities may be used to decrease the computing cost without significantly reducing the accuracy. Note that the current 1D time-space-domain dispersion-relation-based spatial FD can reach $2M$th-order accuracy for 1D acoustic modeling. Similarly, the current 2D time-space-domain dispersion-relation-based spatial FD can reach $2M$th-order accuracy only along eight directions and second-order accuracy along other directions for 2D acoustic modeling (Liu and Sen, 2009c). Therefore, we can use small ε for 1D modeling but large ε for 2D modeling. If a 2D FD scheme to reach $2M$th-order accuracy along all directions is developed in the future, small ε can be used.

The last example of 2D modeling is for the SEG/EAGE salt model. Figure 8 displays snapshots and shot records computed by the FD methods, with fixed and variable FD operator lengths. In the figure, we extend the model spatially to avoid reflections from edges of the model. Figure 8 suggests that FD methods with variable operator lengths are valid for modeling a complex model.

Figure 9 shows FD operator lengths used in Figure 8e and j, demonstrating that the lengths of FD stencils used in Figure 8d and i can be

Table 4. The 2D FD operator lengths $2M + 1$ for different velocities and one maximum frequency used in Figure 7.

		M for different velocities			
f_{max} (Hz)	η	1500 m/s	2000 m/s	2500 m/s	3000 m/s
30	10^{-5}	34	10	6	4

Table 5. CPU time of 2D FD modeling for the horizontal layered model in Figure 7a. Values of $M = 34$, 10, 6, and 4 are used for four different velocities from Table 4.

Type of FD length	Value of M	CPU time of 1000 recursion times (s)
Fixed	34	96.4
Variable	34, 10, 6, 4	68.5

Table 6. The CPU time of 2D FD modeling for different thicknesses. Model parameters are shown in Figure 7a except thicknesses of layers 1 and 6. Values of $M = 34, 10, 6$, and 4 are used for four different velocities from Table 4.

Thickness (m)		CPU time of 1000 recursion times (s)	
Layer 1	Layer 6	Fixed-length method	Variable-length method
2000	1200	96.4	68.5
500	2700	84.6	42.7
100	3100	82.3	28.7

shortened significantly. An average M of 14.2 for the 200×600 grid in Figure 8e is much smaller than a fixed M of 34 used in Figure 8d and i. For 4000 time steps of the 200×600 grid, CPU time on the same laptop computer is 1367.5 and 642.2 s, respectively, for fixed and variable FD operator lengths.

Generally, the stability condition becomes stricter with the increasing FD operator length (e.g., Liu and Sen, 2009c). Therefore, when FD modeling with fixed FD operator length is stable, FD modeling with variable FD operator lengths is also stable because variable lengths are not larger than fixed lengths.

VALIDITY AND ABSORBING BOUNDARY CONDITION

In this section, we study two cases to demonstrate the validity of variation of FD operator length in homogeneous and continuous media. The first case is to study whether variation of operator length in homogeneous media generates observable artificial reflections. The second case is to study whether the variable FD-operator-length method can be used in models with linear velocity variation.

Figure 10a shows a snapshot computed by a fixed-length operator for a homogeneous model, and Figure 10b and c shows snapshots generated by variable-length operator modeling. The operator length changes at a depth of 3000 m, i.e., $M = 10$ is used from zero to 3000 m and $M = 5$ is used from 3020 to 3980 m in Figure 10b, and $M = 3$ in Figure 10c from 3020 to 3980 m. In Figure 10b, it is difficult to identify artificial reflections at the depth where the operator length changes. However, artificial reflections can be seen in Figure 10c.

Next, we investigate the cause of the occurrence of such artificial reflections. We know that reflections occur at the point where medium velocity suddenly changes. In numerical modeling, reflections occur at locations where dispersion velocity suddenly changes. If dispersion velocity changes little within the effective frequency band, then artificial reflections will be very small. In Figure 10b, dispersions caused by two different operator lengths are very close, which leads to very small reflections. In Figure 10c, stronger dispersion can be seen beneath the interface where the operator length changes. Stronger dispersions come from stronger variation of dispersion velocity within the effective frequency band. Therefore, we can see artificial reflections generated by variation of operator length. Figure 10 suggests that the FD operator should be designed to make dispersion very small within the effective frequency band, which can be implemented by criterion 14 or 15.

Figure 11b and c shows snapshots by fixed- and variable-length operators, respectively, for a model containing continuous (linear) velocities (Figure 11a). We can see that Figure 11b looks nearly the same as Figure 11c. Reflections cannot be seen within the area of continuous velocities in Figure 11c. The reason is because for the operator length shown in Figure 11d, dispersion velocity varies slightly with gradual variation of medium velocity.

To study the effectiveness of variable-length-operator-based modeling with the absorbing boundary condition (ABC), we adopt the hybrid ABC (Liu and Sen, 2010b) to reduce boundary reflections caused by a truncated computational domain. The conventional prediction-based ABC predicts boundary wavefield values using approximations such as the one-way wave equation. The hybrid ABC introduces a transition area between the inner area and the boundary to make wavefield values vary smoothly from boundary to inner area via a transition area; thus, absorption effects improve significantly. The hybrid ABC can be used easily to solve a variety of wave-propagation problems numerically.

Figures 12 and 13 show, respectively, 1D records and 2D snapshots computed by (1) fixed-length FD operators without ABC, (2) fixed-length FD operators with the hybrid ABC, and (3) variable-length FD operators with the hybrid ABC for the horizontally layered model. A combination of the variable FD operator length with the hybrid ABC can effectively absorb boundary reflections. Figure 14 shows 2D snapshots for the SEG/EAGE salt model. It also demonstrates the feasibility and validation of combining the variable-length operators with the hybrid ABC.

DISCUSSION

Comparison with variable grid methods

Variable FD-operator-length methods and variable-grid methods reduce computing costs by solving wave equations without significantly reducing accuracy. For low- and high-velocity regions, variable-FD-operator-length methods adopt long and short FD operators, respectively; however, variable-grid methods use small and large grids. Automatic gridding of a velocity model is more difficult than automatically determining operator lengths, especially for complex velocity structures, so variable-grid methods are seldom used in models with complex geology. In addition, some special treatment must be included when waves propagate through small and large grids. However, variable-FD-operator-length methods have been used successfully in complex models such as the SEG/EAGE salt model, and no special treatment is needed when waves propagate through short and long operator grids.

Because FD operator lengths and FD coefficients can be precomputed based on velocity range, grid size, time step, effective frequency band, and accuracy, variable-FD-operator-length methods can be used easily in migration and inversion, based on wave equations and regular grids. However, for variable-grid methods, grids cannot be predivided because of the continuous velocity update in migration and inversion. Therefore, it is difficult to use variable-grid methods in migration and inversion.

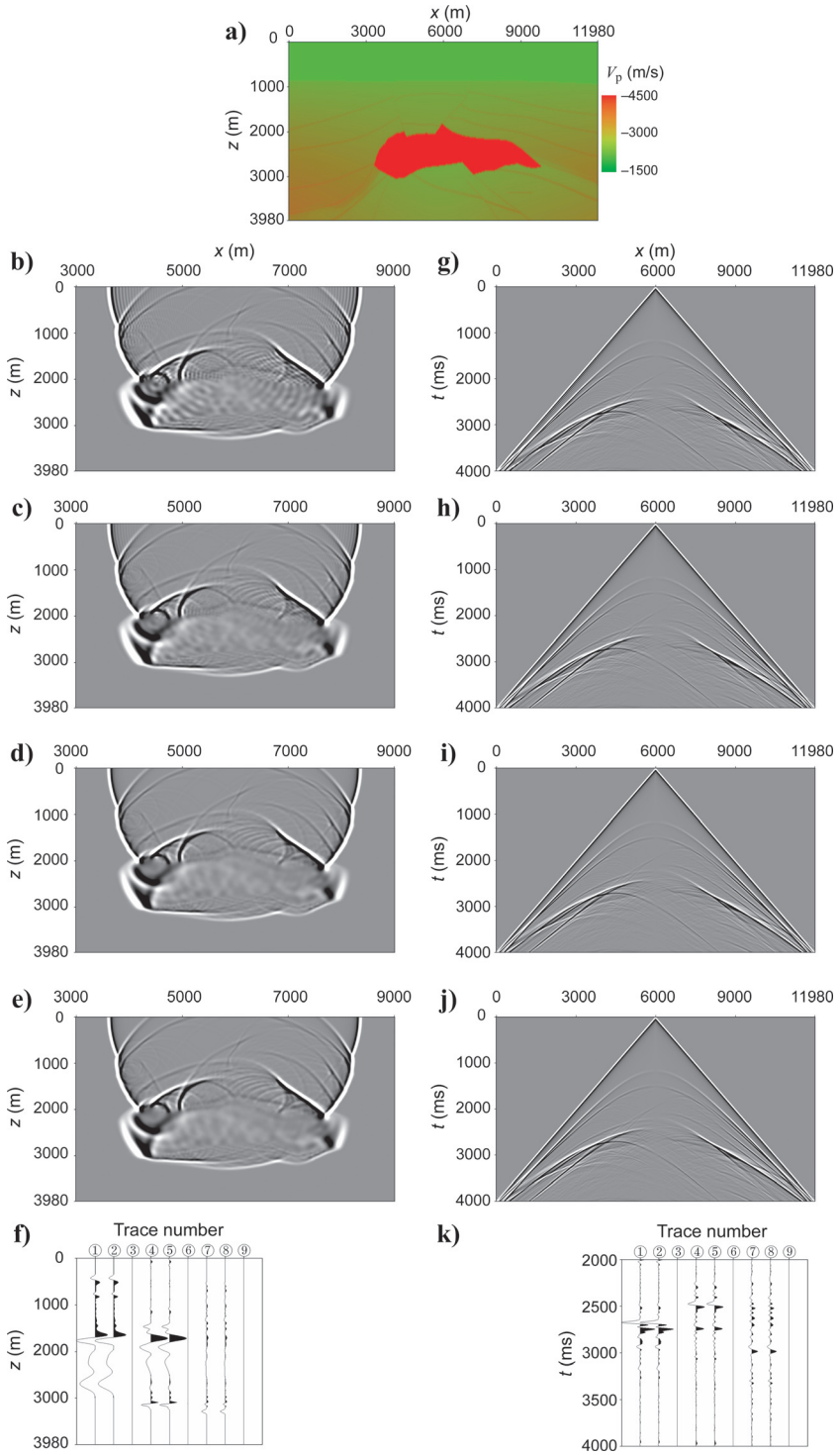

Figure 8. 2D modeling snapshots at 1600 ms and records computed by the FD methods with fixed and variable FD operator lengths for the SEG/EAGE salt model (a). In addition, snapshots computed by fixed-length FD operators with M of (b) 5, (c) 10, and (d) 34. (e) A snapshot computed with variable FD operator lengths, M ranging from 34 to 3. (f) Comparison of traces 1, 4, and 7 from (d) and traces 2, 5, and 8 from (e). (g-i) Records computed by fixed-length FD operators, with M of (g) 5, (h) 10, and (i) 34. (j) Record computed by variable-length FD operators with M from 34 to 3. (k) Comparison of traces 1, 4, and 7 from (i) and traces 2, 5, and 8 from (j). For all views, $h = 20$ m and $\tau = 0.002$ s. Variable FD operator lengths are determined by using $f_{max} = 30$ Hz and $\eta = 10^{-5}$. The source is located at (6000 m, 20 m). A one-period sine function with 20-Hz frequency is used to generate vibrations. The depth of receivers is 0 m. The x-coordinates of traces 1 and 2, 4 and 5, and 7 and 8 are 4000, 5000, 6000 m, respectively. Traces 3, 6, and 9 are the differences between traces 1 and 2, traces 4 and 5, and traces 7 and 8, respectively. Trace balance by maximum amplitude of each trace is used in (g-j).

Comparison with regridding model method

For FD methods with fixed operator lengths, computing requirements may be decreased by reducing the grid size slightly and the FD order. We call this the regridding model method**.** Generally, the computational requirement of FD modeling is directly proportional to FD operator length, and it is inversely proportional to the grid size and time step for the given velocity model, maximum propagation time, maximum frequency, and given modeling accuracy. Sometimes, a long FD operator and large grid size can be adopted to reach the given accuracy using calculations that cost a minimal amount (Liu and Sen, 2009c). In such a condition, the fixed-length FD operator

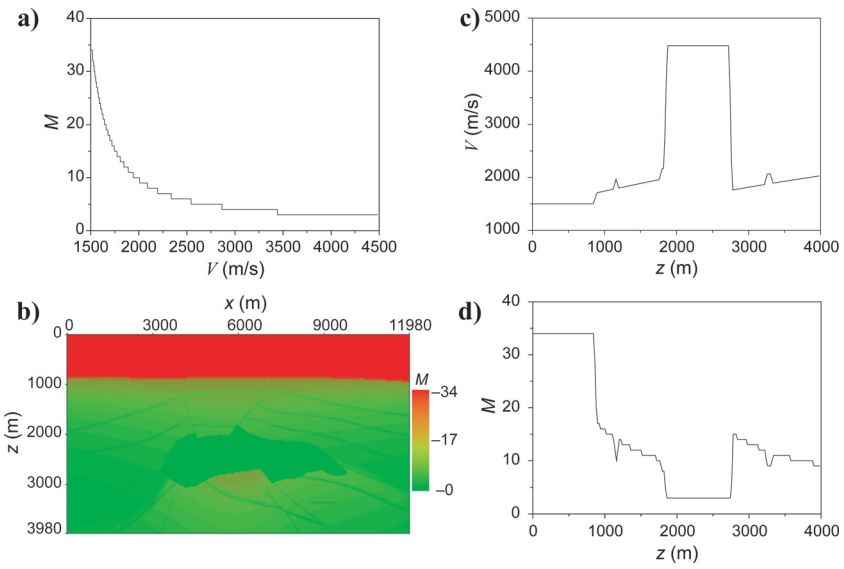

Figure 9. Variable FD operator lengths used in Figure 8e and j. (a) Variation of M with velocity. (b) Variation of M with x and z for the SEG/EAGE salt model. (c) Variation of velocity with z at $x = 6000$ m for the SEG/EAGE salt model. (d) Variation of M with z at $x = 6000$ m for the SEG/EAGE salt model.

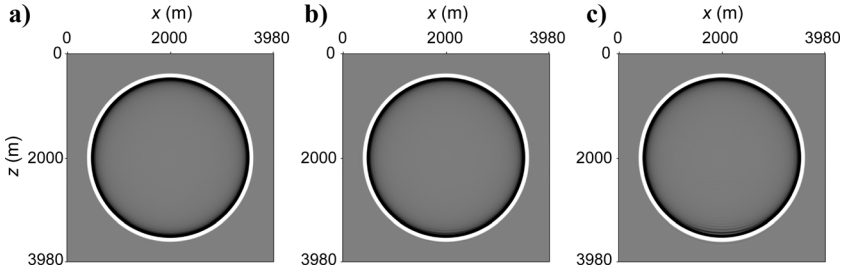

Figure 10. The 2D modeling snapshots at 800 ms, computed by fixed- and variable-length FD operators for a homogeneous model: (a) fixed-length FD operator, $M = 10$; (b) variable-length FD operators, $M = 10$ from 0 to 3000 m and $M = 5$ from 3020 to 3980 m; and (c) variable-length FD operators, $M = 10$ from 0 to 3000 m and $M = 3$ from 3020 to 3980 m. In all snapshots, $V = 2000$ m/s, $h = 20$ m, and $\tau = 0.001$ s.

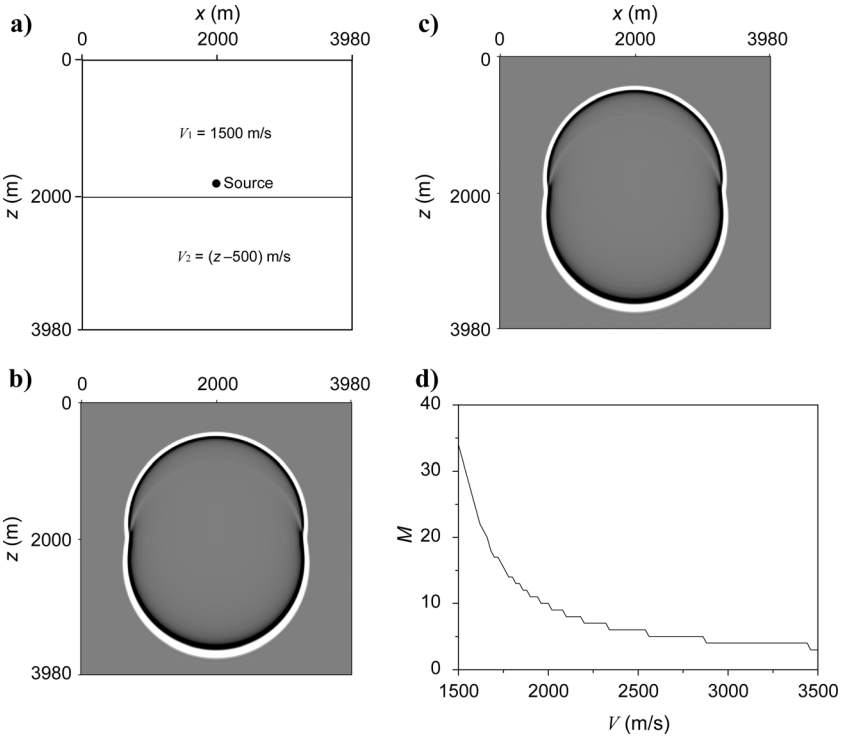

Figure 11. 2D modeling snapshots at 900 ms, computed by fixed- and variable-length FD operators for a horizontally layered model containing continuous (linear) velocities. (a) Model and source," (b) Fixed-length FD operator with $M = 34$, (c) variable-length FD operators with $M = 34$ to 3, (d) variation of M with velocity. In all views, $h = 20$ m and $\tau = 0.001$ s. Variable FD operator lengths are determined by using $f_{max} = 30$ Hz and $\eta = 10^{-5}$.

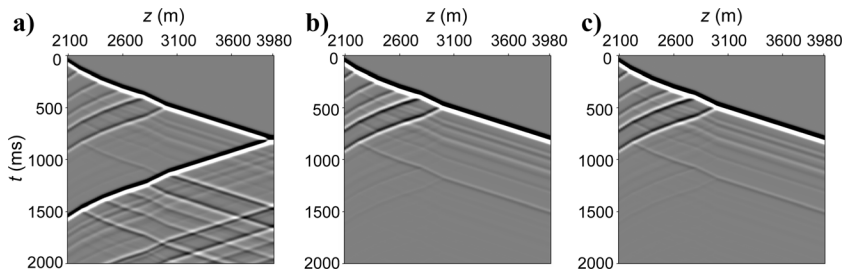

Figure 12. The 1D modeling records computed by (a) fixed-length ($M = 32$) FD operators without ABC, (b) fixed-length FD operators with the hybrid ABC, and (c) variable-length ($M = 32$, 14, 9, and 7 for four different velocities) FD operators with the hybrid ABC for the horizontally layered model. Model and simulating parameters are as those in Figure 6 except receiver depths vary from 2100 to 3980 m. The absorbing boundary layer has a thickness of 10 grids.

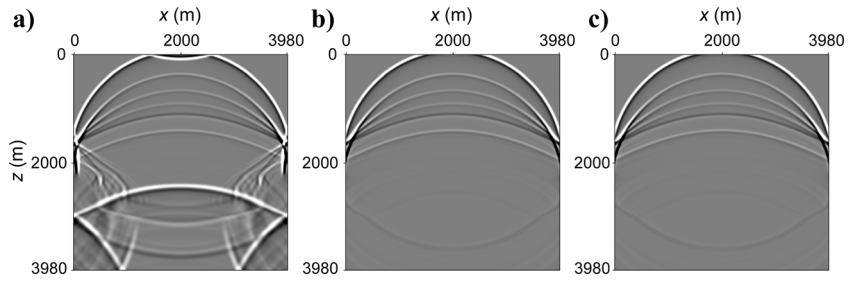

Figure 13. The 2D modeling snapshots at 1400 ms computed by (a) fixed-length ($M = 34$) FD operators without ABC, (b) fixed-length FD operators with the hybrid ABC, and (c) variable-length ($M = 34$, 10, 6, and 4 for four different velocities) FD operators with the hybrid ABC for the horizontally layered model. Model and simulating parameters are as those in Figure 7. The absorbing boundary layer has a thickness of 10 grids.

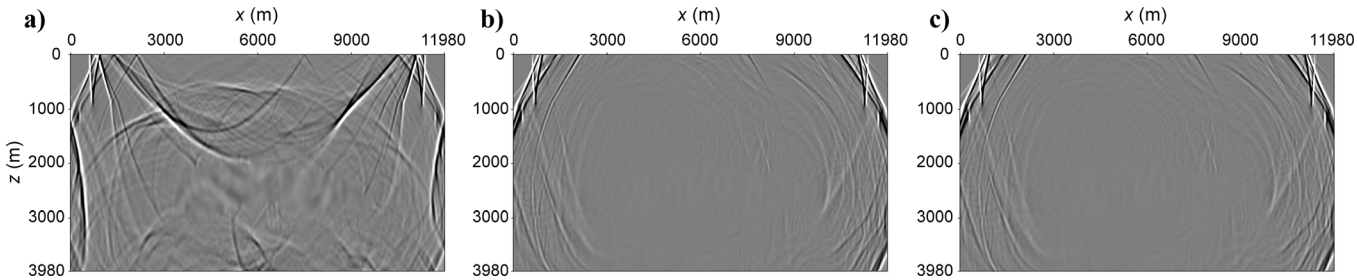

Figure 14. The 2D modeling snapshots at 3600 ms by fixed-length ($M = 34$) FD operators (a) without ABC and (b) with the hybrid ABC and (c) by variable-length (M from 34 to 3) FD operators with the hybrid ABC for the SEG/EAGE salt model. Model and simulating parameters are as those in Figure 8. The absorbing boundary layer has a thickness of 10 grids.

method can be replaced with variable-FD-operator-length methods.

In addition, the accuracy of FD modeling can be improved by decreasing grid size or increasing FD operator length. If the goal is to save memory, increasing FD operator length is preferred over decreasing grid size, especially for 3D modeling. In this case, variable-FD-operator-length methods are preferred.

CONCLUSIONS

We have developed new FD schemes with variable operator lengths. These schemes lead to long operators for low-velocity regions and short operators for high-velocity regions when the grid size and time step are fixed. We have proposed two methods to determine operator lengths for different velocities. The 1D and 2D modeling tests suggest that fixed FD operator length can be replaced by variable FD operator lengths for different velocities to decrease computing cost significantly without reducing accuracy. The hybrid absorbing boundary condition has been combined successfully with our proposed method of variable FD operator lengths. Conventional fixed-length methods may be replaced by our methods for seismic modeling, migration, and inversion to reduce calculation expenses without noticeably decreasing accuracy.

ACKNOWLEDGMENTS

We thank assistant editor Evert Slob, associate editor Stig Hestholm, reviewers Daniel Koehn and Frank A. Maaø, and three anonymous reviewers for constructive criticism of our paper. This research is supported by the National Natural Science Foundation of China (NSFC) under contracts 40839901 and 41074100.

REFERENCES

Abokhodair, A. A., 2009, Complex differentiation tools for geophysical inversion: Geophysics, **74**, no. 2, H1–H11.

Aoi, S., and H. Fujiwara, 1999, 3D Finite-difference method using discontinuous grids: Bulletin of the Seismological Society of America, **89**, 918–930.

Bansal, R., and M. K. Sen, 2008, Finite-difference modelling of S-wave splitting in anisotropic media: Geophysical Prospecting, **56**, 293–312.

Bohlen, T., and E. H. Saenger, 2006, Accuracy of heterogeneous staggered-grid finite-difference modeling of Rayleigh waves: Geophysics, **71**, no. 4, T109–T115.
Claerbout, J. F., 1985, Imaging the earth's interior: Blackwell Scientific Publications, Inc.
Dablain, M. A., 1986, The application of high-order differencing to the scalar wave equation: Geophysics, **51**, 54–66.
Emerman, S., W. Schmidt, and R. Stephen, 1982, An implicit finite-difference formulation of the elastic wave equation: Geophysics, **47**, 1521–1526.
Etgen, J. T., and M. J. O'Brien, 2007, Computational methods for large-scale 3D acoustic finite-difference modeling: A tutorial: Geophysics, **72**, no. 5, SM223–SM230.
Fei, T., and C. L. Liner, 2008, Hybrid Fourier finite-difference 3D depth migration for anisotropic media: Geophysics, **73**, no. 2, S27–S34.
Finkelstein, B., and R. Kastner, 2007, Finite difference time domain dispersion reduction schemes: Journal of Computational Physics, **221**, 422–438.
——, 2008, A comprehensive new methodology for formulating FDTD schemes with controlled order of accuracy and dispersion: IEEE Transactions on Antennas and Propagation, **56**, 3516–3525.
Fornberg, B., 1987, The pseudospectral method — Comparisons with finite differences for the elastic wave equation: Geophysics, **52**, 483–501.
——, 1998, Calculation of weights in finite difference formulas: SIAM Review, **40**, 685–691.
Graves, R. W., 1996, Simulating seismic wave propagation in 3D elastic media using staggered-grid finite differences: Bulletin of the Seismological Society of America, **86**, 1091–1106.
Hayashi, K., and D. R. Burns, 1999, Variable grid finite-difference modeling including surface topography: 69th Annual International Meeting, SEG, Expanded Abstracts, 523–527.
Hestholm, S., 2009, Acoustic VTI modeling using high-order finite differences: Geophysics, **74**, no. 5, T67–T73.
Holberg, O., 1987, Computational aspects of the choice of operator and sampling interval for numerical differentiation in large-scale simulation of wave phenomena: Geophysical Prospecting, **35**, 625–655.
Igel, H., P. Mora, and B. Riollet, 1995, Anisotropic wave propagation through finite-difference grids: Geophysics, **60**, 1203–1216.
Jastram, C., and A. Behle, 1993, Accurate finite-difference operators for modelling the elastic wave equation: Geophysical Prospecting, **41**, 453–458.
Kelly, K. R., R. Ward, W. S. Treitel, and R. M. Alford, 1976, Synthetic seismograms: A finite-difference approach: Geophysics, **41**, 2–27.
Kindelan, M., A. Kamel, and P. Sguazzero, 1990, On the construction and efficiency of staggered numerical differentiators for the wave equation: Geophysics, **55**, 107–110.
Krüger, O. S., E. H. Saenger, and S. Shapiro, 2005, Scattering and diffraction by a single crack: An accuracy analysis of the rotated staggered grid: Geophysical Journal International, **162**, 25–31.
Larner, K., and C. Beasley, 1987, Cascaded migrations — Improving the accuracy of finite-difference migration: Geophysics, **52**, 618–643.
Lele, S. K., 1992, Compact finite difference schemes with spectral-like resolution: Journal of Computational Physics, **103**, 16–42.
Li, Z., 1991, Compensating finite-difference errors in 3-D migration and modeling: Geophysics, **56**, 1650–1660.
Liu, Y., and M. K. Sen, 2009a, A practical implicit finite-difference method: Examples from seismic modeling: Journal of Geophysics and Engineering, **6**, 231–249.
——, 2009b, An implicit staggered-grid finite-difference method for seismic modeling: Geophysical Journal International, **179**, 459–474.
——, 2009c, A new time-space domain high-order finite-difference method for the acoustic wave equation: Journal of Computational Physics, **228**, 8779–8806.
——, 2010a, Acoustic VTI modeling with a time-space domain dispersion-relation-based finite-difference scheme: Geophysics, **75**, no. 3, A11–A17.
——, 2010b, A hybrid scheme for absorbing edge reflections in numerical modeling of wave propagation: Geophysics, **75**, no. 2, A1–A6.
Madariaga, R., 1976, Dynamics of an expanding circular fault: Bulletin of the Seismological Society of America, **66**, 639–666.
Opršal, I., and J. Zahradník, 1999, Elastic finite-difference method for irregular grids: Geophysics, **64**, 240–250.
Pratt, R. G., C. Shin, and G. J. Hicks, 1998, Gauss-Newton and full Newton methods in frequency-space seismic waveform inversion: Geophysical Journal International, **133**, 341–362.
Ravaut, C., S. Operto, L. Improta, J. Virieux, A. Herrero, and P. Dell' Aversana, 2004, Multiscale imaging of complex structures from multifold wide-aperture seismic data by frequency-domain full-waveform tomography: Application to a thrust belt: Geophysical Journal International, **159**, 1032–1056.
Ristow, D., and T. Ruhl, 1994, Fourier finite-difference migration: Geophysics, **59**, 1882–1893.
——, 1997, 3-D implicit finite-difference migration by multiway splitting: Geophysics, **62**, 554–567.
Robertsson, J. O. A., 1996, A numerical free-surface condition for elastic/viscoelastic finite-difference modeling in the presence of topography: Geophysics, **61**, 1921–1934.
Robertsson, J. O. A., J. Blanch, and W. Symes, 1994, Viscoelastic finite-difference modeling: Geophysics, **59**, 1444–1456.
Saenger, E. H., N. Gold, and S. A. Shapiro, 2000, Modeling the propagation of elastic waves using a modified finite-difference grid: Wave Motion, **31**, 77–92.
Tessmer, E., 2000, Seismic finite-difference modeling with spatially varying time steps: Geophysics, **65**, 1290–1293.
Virieux, J., 1984, SH-wave propagation in heterogeneous media: Velocity-stress finite-difference method: Geophysics, **49**, 1933–1957.
——, 1986, P-SV wave propagation in heterogeneous media: Velocity stress finite difference method: Geophysics, **51**, 889–901.
Wang, Y., and G. T. Schuster, 1996, Finite-difference variable grid scheme for acoustic and elastic wave equation modeling: 66th Annual International Meeting, SEG, Expanded Abstracts, 674–677.
Zhang, G., Y. Zhang, and H. Zhou, 2000, Helical finite-difference schemes for 3-D depth migration: 70th Annual International Meeting, SEG, Expanded Abstracts, 862–865.